

A New Broadband Antenna of High Gain: The Double-Cornu Spiral Antenna

Paul Tcheg, Matthias Möck, and David Pouhè*

Abstract—A new planar compact antenna composed of two crossed Cornu spirals is presented. Each Cornu spiral is fed from the center of the linearly part of the curvature between the two spirals, which builds the clothoid. Sequential rotation is applied using a sequential phase network to obtain circular polarization and increase the effective bandwidth. Signal integrity issues have been addressed and designed to ensure high quality of signal propagation. As a result, the antenna shows good radiation characteristics in the bandwidth of interest. Compared to antennas of the same size in the literature, it is broadband and of high gain. Although the proposed antenna has been designed for K- and Ka-band operations, it can also be developed for lower and upper frequencies because of the linearity of the Maxwell equations.

1. INTRODUCTION

Antennas are widely used in high-density wireless communication systems, millimeter-wave radars, satellite communications, sensing systems, and amateur radios. As a core device in these engineering applications, the antenna should fulfill some requirements, including low profile, broadband properties, and circular polarization for applications like satellite communications. One of the most prominent candidates to fulfill these requirements is, among others, spiral antenna. This antenna has been subject to many studies since its design in the 1950s [1, 2, 7]. In its classical geometry, spiral antenna is a self-complementary device consisting of symmetrically spaced arms. The antenna is fed in the center point of the spiral to provide broadband and circular polarisation characteristics. However, like any low-profile single-element antenna, the planar spiral is of poor gain.

Overcoming this “drawback” of the single element antenna is sometimes necessary since in some frequency bands, because of significant atmospheric effects such as absorption and attenuation, e.g., at 60 GHz band and some modern sensing systems, high gain antennas are required. Different techniques can be used to obtain satisfactory antenna characteristics [3, 4]. Amongst these techniques, one approach commonly used to obtain high gain antennas is arranging spaced yet interconnected several single-element antennas to increase the directivity of the radiator. This method is commonly referred to as an array, whose overall gain depends amongst others on the use of relatively high-gain antenna elements.

Drawbacks of antenna arrays reside however in their overall large size, when the number of elements increases and in the existence of side lobes whose reduction requires additional antenna synthesis approaches to obtain optimum results for the given system specifications [3, 4]. Their application is time-consuming.

This paper presents a new family of high gain spiral antenna elements, which may be used either as a single-element antenna or combined into several single-element antennas to form an antenna array. Next to this section, the structure of the antenna is described. As the antenna is sequentially fed,

Received 6 January 2022, Accepted 11 February 2022, Scheduled 25 February 2022

* Corresponding author: David Pouhè (david.pouhe@reutlingen-university.de).

The authors are with the School of Engineering, Reutlingen University of Applied Sciences, Alteburgstrasse 150, D-72762 Reutlingen, Germany.

Section 3 deals with the feeding network. Simulated results are presented and discussed in Section 4. Section 5 compares experimental and simulated data.

Given that the nature of the engineering sciences is the enlightening of scientific realizations with respect to their technical applicability and practical conversion, proper due is given throughout the work to the manufacture requirements for production purposes of the antenna.

2. THE ANTENNA STRUCTURE

2.1. Structure and Description of the Radiating Element

Figure 1 is a plan and a 3D-view showing that the planar Cornu-Spiral antenna is patterned on a dielectric substrate of permittivity $\varepsilon_r = 3$ and height 1.5 mm over a ground plane to ensure unidirectional operation. The dielectric acts as a supporting material. The Cornu-Spiral antenna herein described consists of two elongated electrically conductive elements wound, each into an equiangular/archimedean spiral. It has two central ends and is cut in the middle of its central linear part into two parts to create a delta gap for feeding purposes (Fig. 1(a)), thus forming two separated coplanar spirals lying in two diametrically opposite quadrants. That is, the second spiral is obtained upon rotating the first spiral by an angle of $\pm\pi$ about the z -axis. Each spiral arm is designed to radiate the axial mode at least at the operation frequency and exhibits broadband attributes. It has two ends: a central end and an outer end. The central ends are aligned along the same diagonal. Note that the definition of central and outer ends is according to the classical definition of spiral antennas' central and outer ends.

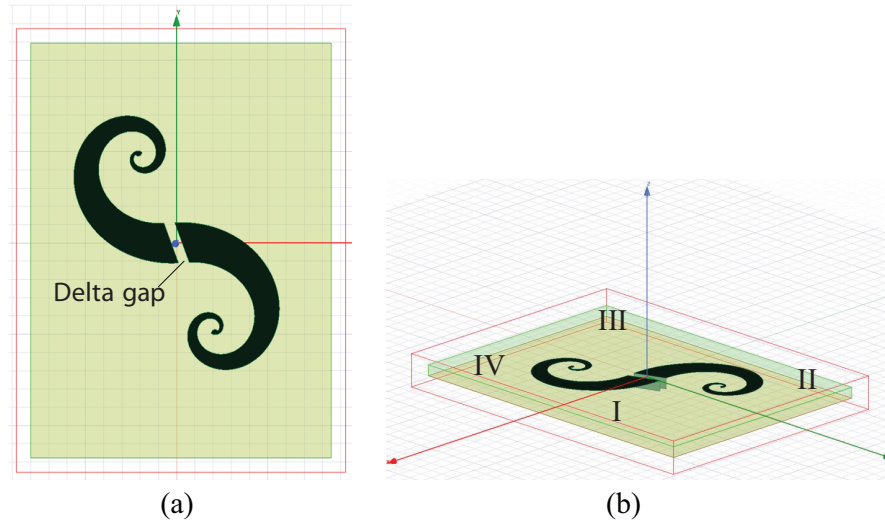


Figure 1. The Cornu-Spiral antenna. (a) Plan view and (b) 3D-view.

Since the designed arm is intended to radiate the axial mode and due to the conceptual similarity between the conical helix antenna and the wounded parts of the cornu antenna [5, 6], the condition $0.8\lambda < \pi D < 1.3\lambda$ is applied on the design of the core element of the Cornu spiral antenna.

The wideband attributes required for the designed arm depend mainly on the number of turns NT ; its value should therefore be carefully chosen. To design an optimum low-size spiral antenna for the given requirements, the parameter NT should be larger than 1 but smaller than 2. To that end and to simplify the investigations processes, NT is set to 1.6.

The requirements above imply that the arm growth a and the number of turns NT are the main parameters for designing the arm. During the first stage of the development of the arm, a large number of structures were designed and investigated. The arm growth was varied by 0.05 step from 0.1 to 0.4. It was found that with an arm growth of 0.1, the spiral radiates an axial mode over a large frequency band around the operation frequency of 24 GHz when currents on the arm, included in the πD -circle,

are in phase as demonstrated by Bawer and Wolfe in [7]. However, as it is intended to interconnect the antenna to its feeding network through signal vias embedded into a dielectric material (Sections 2.2 and 2.3) and because of manufacture requirements, we then decided to disregard the option with an arm growth $a = 0.1$ and chose $a = 0.35$ (while maintaining the number of turns unchanged) in order to match the manufacture requirements by keeping broadband characteristics of the antenna.

Indeed, the input impedance of a spiral with an arm growth $a = 0.1$ over a dielectric of permittivity $\epsilon_r = 3$ is nearly 137Ω , a value which is more significant than the required value of 65Ω . A significantly high input impedance value would lead to a small diameter of vias that cannot be manufactured as an aspect ratio of $1 : 8$ is necessary to drill holes for a blind via corresponding to the minimum achievable diameter [8]. The total thickness of the PCB, which includes a large part of the antenna’s substrate and the feed’s substrate, determines the needed diameter. Details on this issue are provided in the next section.

Figure 2 shows the input impedance of a spiral arm with an arm growth of 0.35. As can be seen, the impedance has nearly a constant value of 65Ω over a large frequency band. Although not presented here because of space limitation, the wounded microstrip trace radiates an axial mode over a wide frequency band.

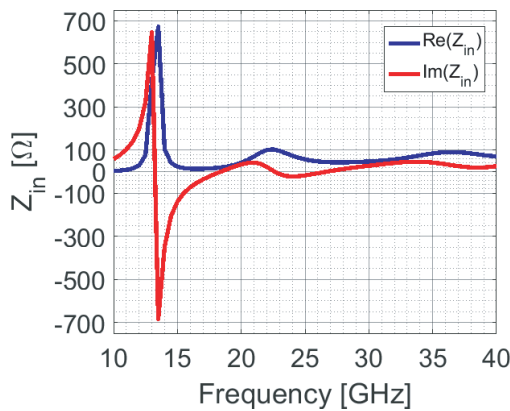


Figure 2. Input impedance of a spiral arm with an arm growth of 0.35.

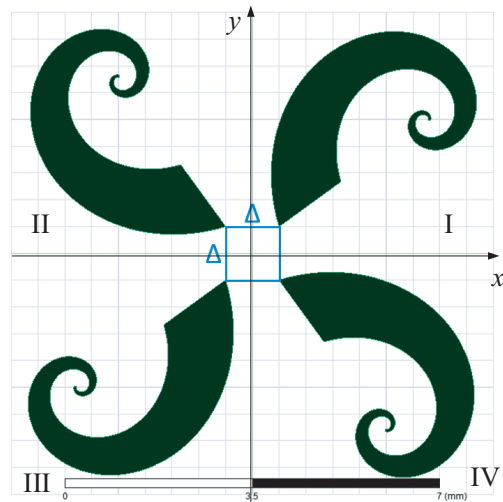


Figure 3. Plan view of the Double Cornu-Spiral antenna. As can be seen, each spiral lies in one quadrant.

Note that increasing the arm growth while keeping the number of turns, NT , unchanged maintains the axial mode’s radiation at 24 GHz and over a larger frequency band around the operation frequency. In addition, the value of the input impedance can be improved to the desired one.

By mounting a second clothoid rotated by an angle of $\pm \frac{\pi}{2}$ about the z -axis close to the first, the double Cornu-spiral antenna (DCSA) consisting of four coplanar spiral arms is obtained (Fig. 3). The central ends of two diametrically opposite spirals lie on the same diagonal. That is, each of the four spirals lies in one quadrant. The arm growth of each spiral is $a = 0.35$. A Cornu-Spiral antenna with conductive elements wound into an archimedean spiral can also be realized. However, for the reasons above, we chose equiangular spirals.

The designed spiral arm exhibits wideband characteristics but does not provide circular polarisation. To obtain circular polarisation, we then applied the sequential rotation technique by feeding the antenna elements with equal power but a progressive phase of 90° . Figs. 4 and 5 show obtained results. As can be seen, the antenna exhibits good circularly polarized characteristics.

The results presented here are for ideal feeding. This feeding art belongs fortunately to the so-called academic construct. In most practical cases, however, transmitting power from a transmitter into an antenna or from an antenna into a receiver is achieved through a transmission line and generally

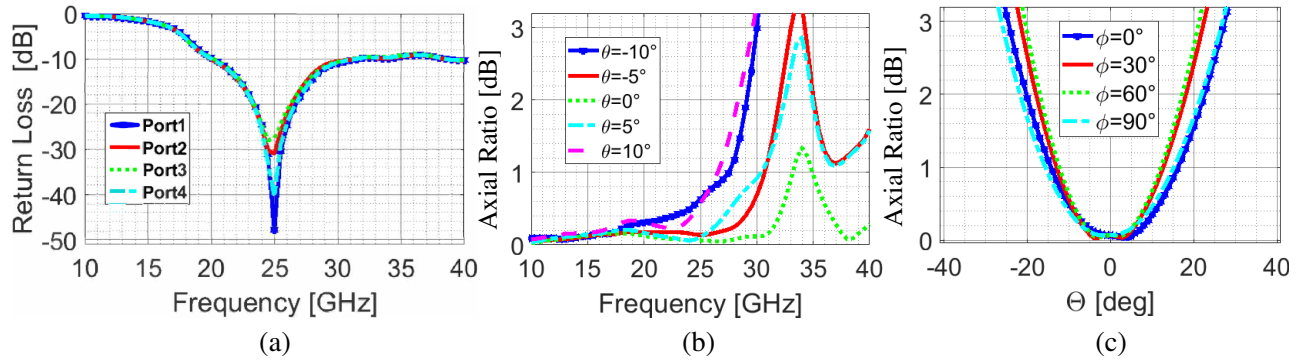


Figure 4. (a) Return Loss, (b) axial ratio as a function of the frequency and (c) versus the elevation of the Double Cornu-Spiral antenna fed ideally.

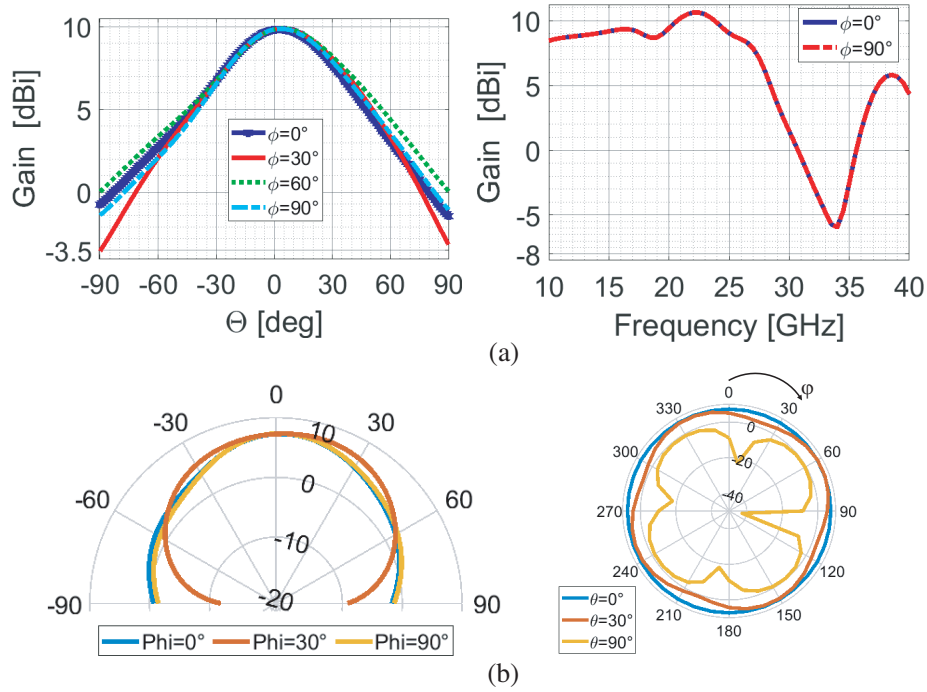


Figure 5. (a) Gain and (b) radiation patterns at $f = 24$ GHz of the double Cornu-spiral antenna with an ideal feed.

requires a feeding network to make optimal use of the available power. The design and description of this network is the subject of the next section.

2.2. The Feeding Network

Contrary to the general case, which consists of feeding a spiral antenna using a tapered [9] or bazooka balun [10, 11], the antenna herein is fed using an integrated wideband stripline sequential phase network (SPN). The SPN is a compact five ports series power divider, whereby port 0 is the input port, and ports 1 to 4 are output ports coupled to the respective radiating element through connecting vias. It is designed following the procedure described in [12, 13] by considering manufacture requirements and the fact that the SPN is embedded into a substrate [14]. The input power P_0 is split into the arms with equal amplitude and appropriate phase to produce various radiation modes. That is, neglecting power losses, the generic power distribution P_i , $i = 1, 2, 3, 4$, among the output ports is $P_0/4$.

Depending on the operation mode needed, the SPN provides either a 90° or 180° phase shift between two adjacent arms. For operation in axial mode, also known as mode M1, the phase shift is 90° , and for mode M2, it is 180° between two adjacent arms. The antenna can also operate in a third mode M3. To that end, the phasing element may be selected to provide a phase shift of 90° between two adjacent arms in the counter-clock sense. A corporate feed can also be used instead with similar results, but with high losses [15].

For the mode M1 operation, Fig. 6 shows a schematic of the designed power divider for a right-hand circular polarization and its equivalent circuit. It has an octagon shape and consists of 7 phase shifters and power dividers operating as quarter-wave transformers whereby the lines with lengths l_1, l_2, l_3, l_4 are adapted lines with corresponding characteristic impedance Z_1, Z_2, Z_3, Z_4 . The remaining quarter-wave transformer lines are of impedances $Z_5, Z_6,$ and Z_7 . l_0 and Z_0 are respectively the length and characteristic impedance of the input line. $Z'_1, Z'_2, Z'_3,$ and Z'_7 represent the impedances when looking at the node or junction in the direction of the marked red arrow.

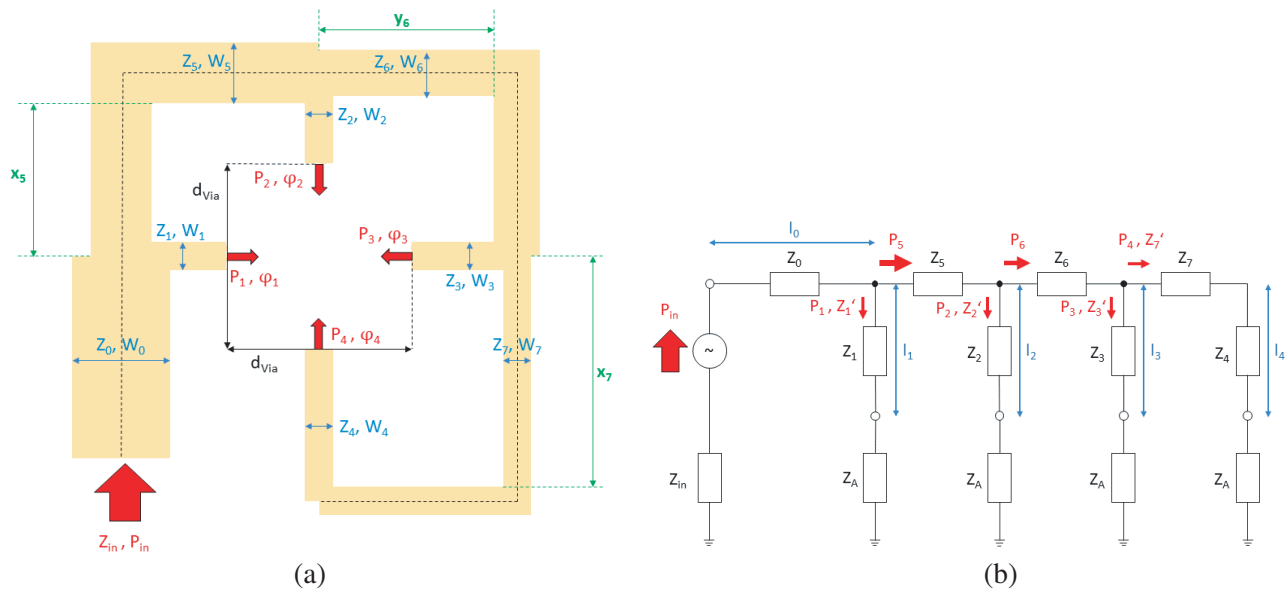


Figure 6. Schematic representation of (a) the designed power divider and (b) its equivalent circuit. The circuit is designed after [12] and [13].

At junctions, the required power and respective impedances in the parallel circuit can be related to each other as:

$$\frac{P_5}{P_1} = \frac{Z'_1}{Z_5} = 3, \tag{1a}$$

$$\frac{P_6}{P_2} = \frac{Z'_1}{Z_6} = 2, \tag{1b}$$

$$\frac{P_4}{P_3} = \frac{Z'_3}{Z'_7} = 1. \tag{1c}$$

Furthermore, impedance matching is ensured by dimensioning the parallel circuit as follows:

$$\frac{1}{Z_0} = \frac{1}{Z'_1} + \frac{1}{Z_5}, \tag{2a}$$

$$\frac{1}{Z_5} = \frac{1}{Z_2} + \frac{1}{Z_6}, \tag{2b}$$

$$\frac{1}{Z_6} = \frac{1}{Z_3} + \frac{1}{Z'_7}. \tag{2c}$$

From Eq. (1a), we have

$$Z'_1 = 3Z_5. \quad (3)$$

Replacing Z'_1 in Eq. (2a) by its expression from Eq. (3) and solving the obtained equation for Z_5 , we get

$$Z_5 = \frac{4}{3}Z_0. \quad (4)$$

Z_5 can now be set in Eq. (3) to obtain

$$Z'_1 = 4Z_0. \quad (5)$$

The remaining impedances can be calculated similarly, and we obtain $Z_6 = 2Z_0$ and $Z'_2 = Z'_3 = Z'_7 = 4Z_0$.

Since the impedance matching should prevail between the SPN outputs and signal vias and spiral arms, the impedance at feeding outputs should be 65Ω . Hence, $Z_1 = Z_2 = Z_3 = Z_4 = 65 \Omega$. The impedances Z_1, Z_2, Z_3 , and Z_4 are related to Z'_1, Z'_2, Z'_3 , and Z'_7 through the well-known transformation equation from the transmission line theory for the quarter-wave impedance transformer.

From the above procedure, it follows that, if Z_0 is known, all other impedances are obtained. This method is the forward approach since the SPN is dimensioned from the input towards the outputs. Reciprocally, if the output impedances are known, all other impedances can be calculated. Therefore, this approach is named the backward methodology. We applied the last method to dimension the SPN. Obtained characteristic impedances and respective width of the traces are displayed in Table 1. Since the value of Z_0 considerably differs from the generator impedance, 50Ω , it was further transformed through the quarter-wave impedance transformer into an input impedance $Z_e = 50 \Omega$. The rest of the design follows the methodology presented in [14].

Figure 7 shows the SPN with an input impedance of 50Ω . Five shorting pins have been added in the middle to suppress mutual coupling between the different output ports and stabilize thereby the impedance and insertion loss as well. Their position was found empirically upon analysis of electromagnetic field distribution within the substrate. The return loss and insertion loss of the designed feeding network are depicted in Fig. 8. The wideband characteristic of the structure related to the impedance matching can be well appreciated. From 14.21 GHz to 27 GHz, i.e., over a bandwidth of 12.79 GHz, the percentage of the reflected power is maximal 10%. Consequently, the return loss bandwidth intersects that of the DCSA in a broad frequency range. The insertion loss is nearly stable over a large bandwidth. Its values vary between -7.5 and -5 dB around the targeted value of -6.02 dB. Table 2 summarizes obtained results for the return loss, insertion loss, and phase shift between two consecutive arms.

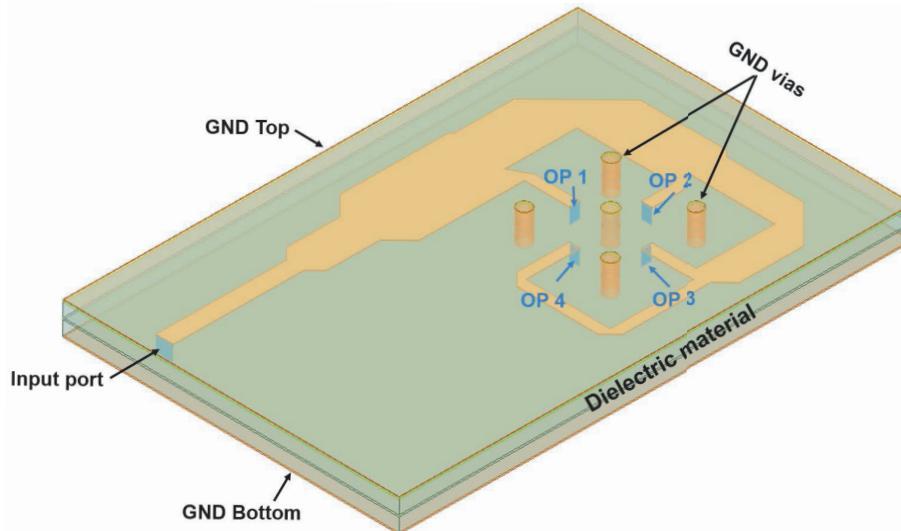


Figure 7. Final designed integrated wideband stripline sequential phase network.

Table 1. Calculated impedances and related trace's width.

| Impedance | Value in [Ω] | Trace's Width in [μm] |
|-----------|-----------------------|------------------------------------|
| Z_e | 50 | 485 |
| Z_L | 28.5 | 1103 |
| Z_0 | 16.25 | 2180.5 |
| Z_1 | 65 | 300 |
| Z_2 | 65 | 300 |
| Z_3 | 65 | 300 |
| Z_4 | 65 | 300 |
| Z_5 | 21.67 | 1552.5 |
| Z_6 | 32.5 | 925 |
| Z_7 | 65 | 300 |

Table 2. Return loss, insertion loss and phase shift between two consecutive arms at 24 GHz.

| Parameter | Value | Parameter | Value |
|---------------------|-----------|-------------------------|-----------|
| Impedance bandwidth | 14.15 GHz | RL | -23.22 dB |
| $S_{1,in}$ | -7.75 dB | $\varphi_2 - \varphi_1$ | 89.69° |
| $S_{2,in}$ | -7.38 dB | $\varphi_3 - \varphi_2$ | 89.39° |
| $S_{3,in}$ | -5.99 dB | $\varphi_4 - \varphi_3$ | 90.45° |
| $S_{4,in}$ | -6.21 dB | $\varphi_1 - \varphi_4$ | 90, 47° |

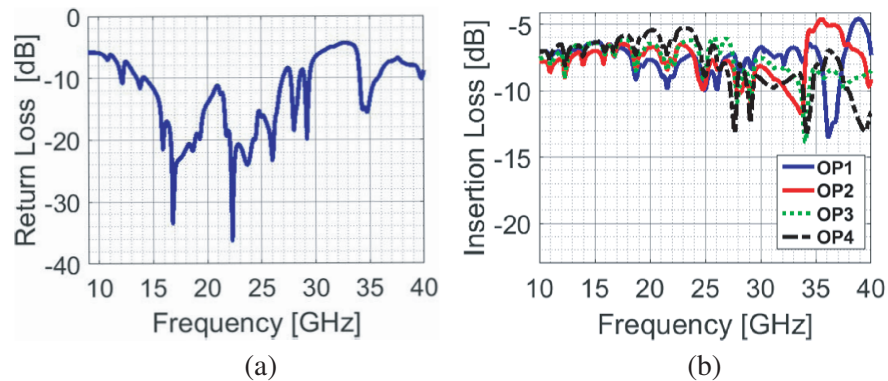


Figure 8. (a) Return Loss and (b) transmission factors of the SPN.

2.3. The Assembled Structure

Having designed the radiating element and feed, we now proceed with the investigation of the combined structure.

Figure 9 shows a 3D-view of the assembled structure composed of the combination of the radiating elements and SPN. As for the previous structures in Subsections 2.1 and 2.2, it has been simulated using ANSYS-HFSS Version 2021 R1, whereby the DCSA has been rotated on the xy -plane around the z -axis by $\pm 90^\circ$ to ensure the alignment between the upper corners inner ends of the DCSA and the pads located at feed's outputs. In addition, the dimensions of the substrate below the DCSA were

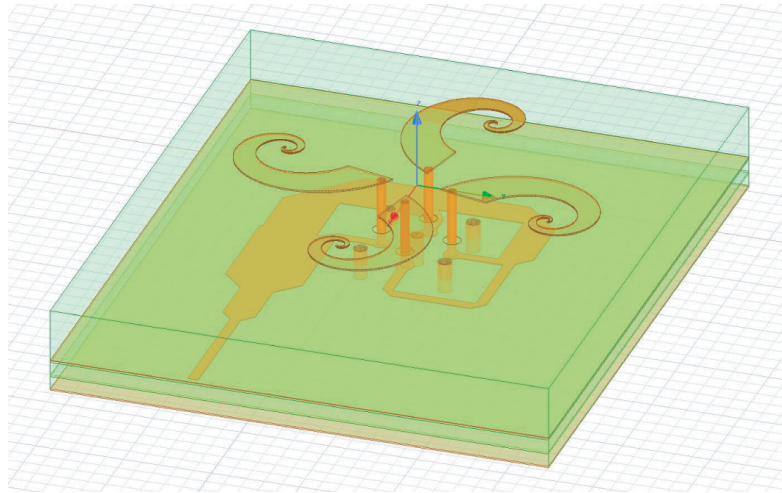


Figure 9. 3D representation of the double cornu-spiral antenna fed with sequential phase network.

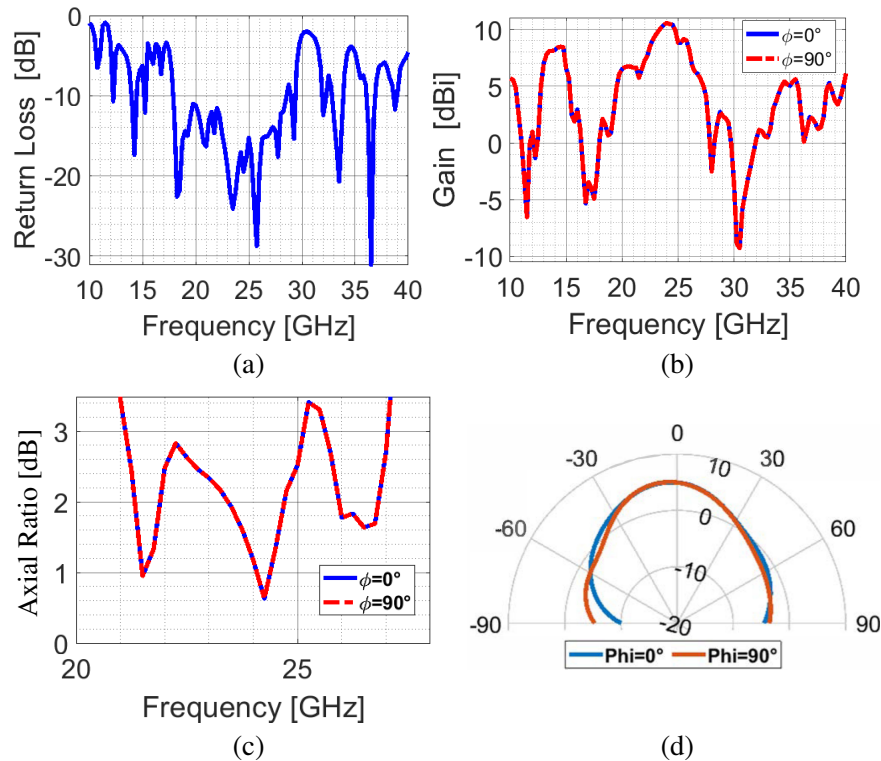


Figure 10. (a) Return loss, (b) gain, (c) axial ratio versus the frequency and (d) *E*-plane radiation pattern of the single element antenna fed with an integrated SPN.

adjusted to match those of the feeding network. Obtained results are displayed in Fig. 10 as presented: The overall impedance bandwidth and effective bandwidth are reduced compared to that with an ideal feed. The antenna still exhibits good radiation characteristics, as expected. The antenna now has an impedance bandwidth of 9.90 GHz instead of 11.33 GHz in the ideal case. The reduction of the operation bandwidth and effective bandwidth is mainly due to ohmic and dielectric losses within the substrate.

We also notice a shift of the frequency range to low frequencies (below 20 GHz). The high return loss quality of the SPN at low frequencies probably has a positive impact in the form of an averaging

effect at the arms input, thus leading to overall good matching conditions. The upper-frequency limit to frequencies below 30 GHz is its side due to the limitation of the SPN at high frequencies.

The antenna shows circular polarization over a bandwidth of about 5.94 GHz which is its effective bandwidth for $\vartheta = 0^\circ$ and $\varphi = 0^\circ$. In this frequency band, the gain is greater than 5 dBi with a maximum of 10.85 dBi at the operating frequency (Fig. 10). The radiation pattern in the E -plane at the operation frequency (Fig. 10) shows that the antenna radiates an axial mode. The asymmetry observed in the pattern is due to the asymmetry of the feeding network and the radiating elements on the board with respect to the yz -plane.

3. EXPERIMENTAL VALIDATION

A prototype of the proposed antenna was manufactured as designed in the previous sections. In addition, connection to the network analyzer through a cable was ensured by mounting a coaxial K-connector at the connection point to the SPN. The manufactured antenna is displayed in Fig. 11. Its layer stack structure is the same as that of the planar equiangular spiral antenna (PESA) presented

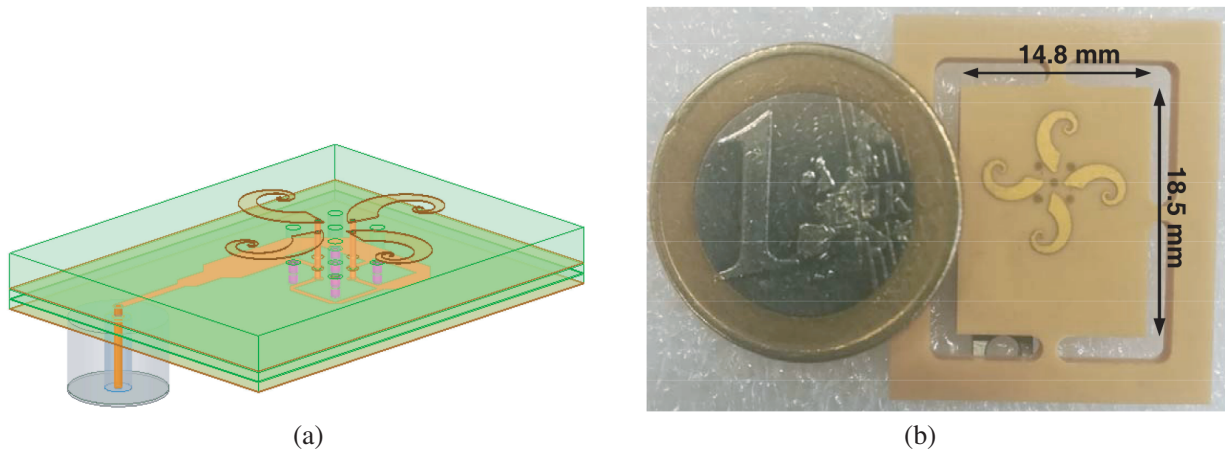


Figure 11. (a) Structure and (b) prototype of the fabricated antenna.

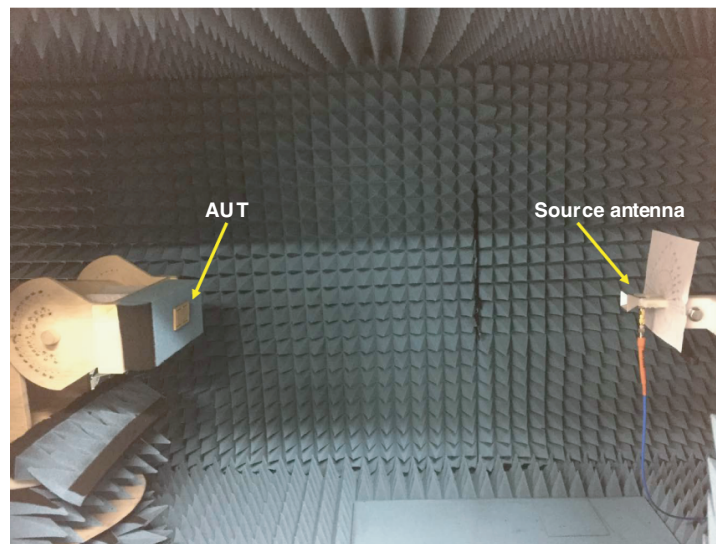


Figure 12. Measurement setup.

in [14, 16] and will therefore not be reproduced here. The antenna has the following overall dimensions: $18.5 \times 14.8 \times 2.453$ mm.

Comparisons between simulations and measurements are shown in Figs. 13 to 15, where the return loss, gain, axial ratio, and radiation patterns for different frequencies are portrayed. Experimental data were obtained throughout this work using an in-house made far-field antenna measurement system consisting of a full-anechoic chamber operating from 3 to 80 GHz (Fig. 12), a linearly polarized standard gain horn antenna, with a constant gain of 13 dB from 17 to 34 GHz, and a network analyzer (R&S ZNB). The measurement step was 50.0 MHz for frequencies and 5° for the elevation angle.

Compared to the case without connector, i.e., the case of Fig. 10 with a lumped port at the input, the manufactured antenna shows a reduced impedance bandwidth due to reflections at the junction between the coaxial connector and the stripline. In fact, since the ground plane around the center pin has been cleared, the impedance between the center conductor and the edge of stripline ground plane

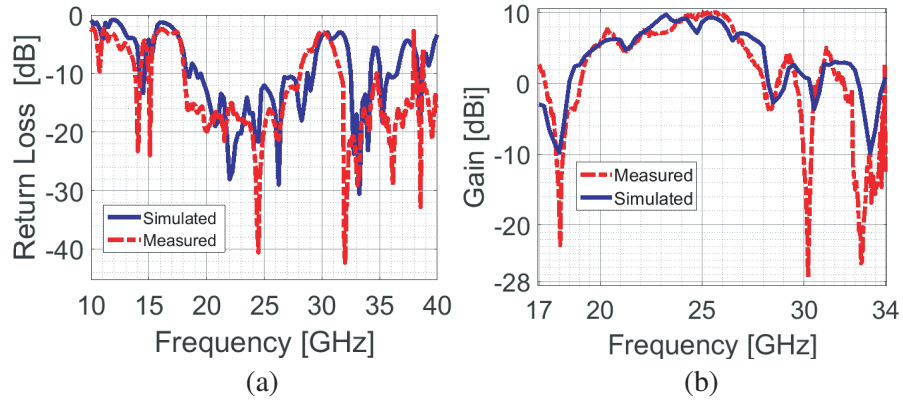


Figure 13. Comparison between full-wave and experimental data. (a) Return loss and (b) gain versus frequency.

Table 3. Summary of obtained results from simulation and measurements.

| Parameter | Simulated | Measured |
|--|---|--|
| Impedance bandwidth | 9.7 GHz & 1.7 GHz (19.5–29.2) GHz & (32.5–34.2) GHz | 10 GHz & 7.3 GHz (18–28) GHz & (31.7–38) GHz |
| RL @ 24 GHz | −17.5 dB | −27.43 dB |
| Max. Gain | 9.85 dBi @ 23.25 GHz | 9.65 dBi @ 25.7 GHz |
| Gain (@ $\vartheta = 0^\circ$, and $f = 24$ GHz) | 8.85 dBi | 8.65 dBi |
| ABW (@ $f = 24$ GHz, $\varphi = 0^\circ$) | 29.5° (-17.5° to $+12^\circ$) | 14.5° (-12° to $+2.5^\circ$) |
| EBW | 4.3 GHz (22–26.3) GHz | 4.5 GHz (22–26.5) GHz |
| Cross-Pol. level @ $\vartheta = 0^\circ$ (@ $\varphi = 0^\circ$; $\vartheta = 90^\circ$) | −19.8 dB | −18.7 dB |
| Max. Cross-Pol. level (@ $\varphi = 0^\circ$; $\varphi = 90^\circ$) | −30.4 dB | −23.02 dB |

has become undefined, resulting thus in an abruptly flow of the signal current from the center pin to the stripline layer [14]. In addition to that, the intersection region between the vertical center conductor and the stripline acts as an antenna, since electric charges moving at uniform velocity along a bent conductor accelerate and radiate.

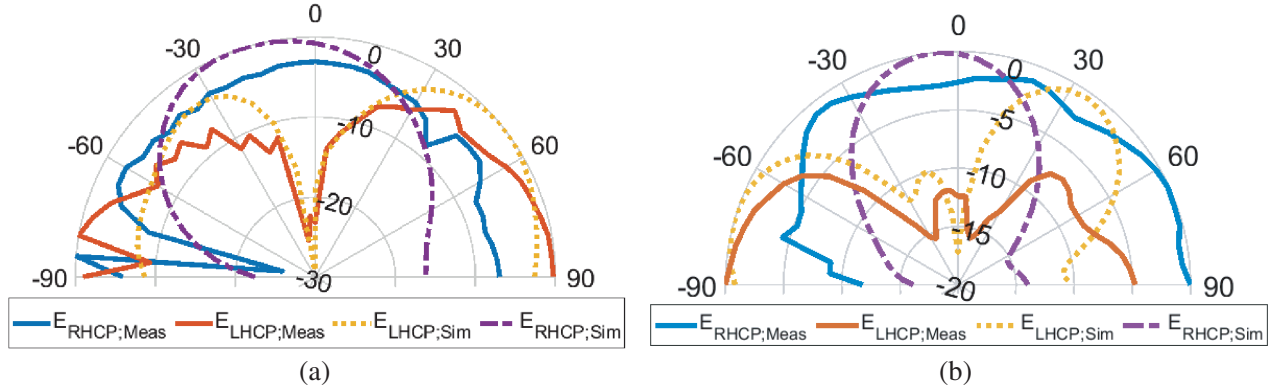


Figure 14. Comparison between full-wave and experimental data. Co- and cross-polarization components (a) at $\phi = 0^\circ$ and (b) at $\phi = 90^\circ$.

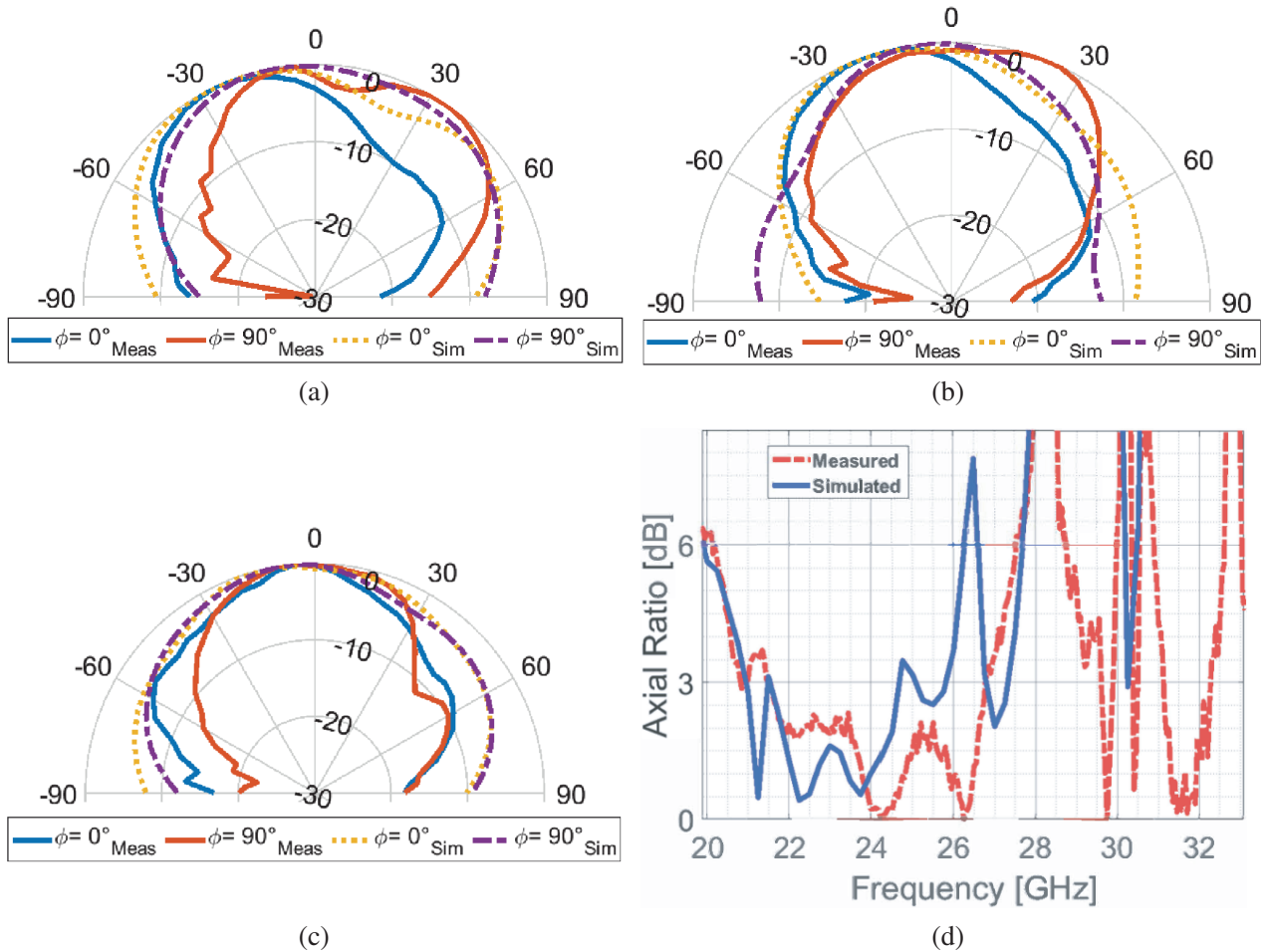


Figure 15. Radiation pattern at (a) 22 GHz, (b) 24 GHz, (c) 26 GHz and (d) axial ratio versus frequency.

Sources of errors such as misalignments of the AUT in the chamber, measurement uncertainties, inaccuracies in soldering the pin connector, manufacturing tolerances, human-made noise, etc., being considered, the consistency between simulation and experiments can be well appreciated by comparing obtained results. Experimental data corroborate full-wave simulations over the considered frequency range. Some characteristics such as the return loss and axial ratio of the fabricated antenna are even better than simulations (Figs. 13–14 and Table 3).

The fabricated antenna even performs better at some frequencies than the simulated one. The manufactured antenna has an impedance bandwidth of over 16 GHz subdivided into two frequency bands: from 18 GHz to 28.02 GHz and 31.75 GHz to 38 GHz. On the other hand, the simulated antenna shows a return-loss bandwidth over 13 GHz ranging from 19.5 GHz to 29.3 GHz, from 32.5 GHz to 34.2 GHz, and a narrow band from 35 GHz to 36.5 GHz. A similar trend is observed for the axial ratio.

The antenna is right-hand circularly polarized (RHCP) with a high degree of polarization purity over a large bandwidth, as can be seen in Fig. 14. The discrepancies between measurements and simulations in the radiation pattern are most likely due to human-made noise and measurement uncertainties. Our measurement setup suffers from one drawback: it is not automated. The AUT is rotated manually. This fact makes angular misalignments between the transmitting and receiving antennas very likely.

The proposed antenna does not need to fear any comparison with existing antennas of the same sizes (or nearly) in the literature as can be seen from Table 4, where radiation characteristics of the DSCA are compared with those of some similar antennas [12, 14, 17, 18]. The DSCA performs favorably.

Table 4. Performance comparison with some existing antennas in the literature.

| Antenna type and Ref. | Single PESA [14] | A Ka-Band High-Gain [12] | Low-Profile Circularly [17] | 2 × 2 Slot Spiral Cavity [18] | This work |
|-----------------------|--------------------------------|------------------------------------|-----------------------------|--|---------------------------------|
| Technology | Stripline | Microstrip + Sequential rotation | SIW + Sequential rotation | Printed gap waveguide + Sequential rotation* | Stripline + Sequential rotation |
| Type of Element | Patch spiral | Patch | Cavity-backed slot | Slot spiral | Patch spiral |
| Number of elements | 1 | 4 (2 × 2 Array) | 4 (2 × 2 Array) | 1 (selected) | 1 |
| Feed Location | Layer under radiating elements | Same layer with radiating elements | under slot /substrate | Layer under radiating elements | Layer under radiating elements |
| Dimensions [mm] | 10 × 7 × 3.2 | 16 × 16 × 0.254 | 38.5 × 38.5 × 1.07 | 7.4 × 7.4 × 2.028 22.9 × 22.9 × 2.028* | 18.5 × 14.8 × 2.453 |
| Op. Frequency [GHz] | 24 | 29 | 28 | 38 | 24 |
| Impedance BW [GHz] | 7.6 + 3.4 = 11 | 4.59 | 6.35 | 5.76 (simulated) | 10 + 7 = 17 |
| AR BW [GHz] | 4.2 | > 1.55 | 1.95 | 0.63 (simulated) 8.75* | 4.5 |
| Peak Gain [dBi] | 9.65 | 13.59 | 7.77 | 4.9 (simulated) 9.3* | 9.65 |

* valid for the array.

4. CONCLUSION

A new family of circularly polarized broadband antennas has been presented. The antenna comprises two Cornu-spirals rotated by an angle of $\pm\pi/2$ about the axis perpendicular to the antenna plane. The sequential rotation technique is used to obtain circular polarization. To that end, a hybrid ring feeding network embedded into the dielectric was designed and integrated with the radiating elements to obtain a compact antenna of small size. Signal integrity issues have been addressed and designed to ensure high quality of signal propagation. The proposed antenna shows good radiation characteristics in the frequency band of interest and is of high gain compared to antennas with the same dimensions in the literature. Predicted and experimental results are in close agreement.

Although being designed for K- and Ka-band, the new antenna can also be constructed for operation in other frequency bands. Arrays of double Cornu-spiral antennas can also be designed, as will be shown in an upcoming study.

ACKNOWLEDGMENT

The authors would like to thanks Mr. Nicolo Randazzo from Rohde & Schwarz in Munich for having provided the ZNB network analyzer for measurements.

REFERENCES

1. Chatterjee, J. S., "Radiation field of a conical helix," *Journal of Applied Physics*, Vol. 24, No. 5, 550–559, May 1953.
2. Turner, E. M., "Spiral slot antenna," *U.S. Patent 2,863,145*, Dec. 1958.
3. Stutzman, W. L. and G. A. Thiele, *Antenna Theory and Design*, 2nd Edition, John Wiley & Sons, New York, 1998.
4. Balanis, C. A., *Antenna Theory. Analysis and Design*, 513–514, 3rd Edition, John Wiley & Sons, New York, 2005.
5. King, H. E. and J. L. Wong, "Helical antennas," *Antenna Engineering Handbook*, R. C. Johnson, McGraw-Hill, New York, 1993.
6. Duhamel, R. H. and J. P. Scherer, "Frequency independant antenna," *Antenna Engineering Handbook*, R. C. Johnson, McGraw-Hill, New York, 1993.
7. Bawer, R. and J. J. Wolfe, "The spiral antenna," *IRE International Convention Record*, 84–95, 1958.
8. http://www.contag.de/uploads/pi_ti/technische_ausfuehrung.pdf.
9. Vinayagamorthy, K., J. Coetzee, and D. Jayalath, "Microstrip to parallel strip balun as spiral antenna feed," *Proc. of the IEEE 75th Vehicular Technology Conference, IEEE, Intercontinental Yokohama Grand, Yokohama*, May 2012.
10. Bawer, R. and J. J. Wolfe, "A printed circuit balun for use with spiral antennas," *IRE Transactions on Microwave Theory and Techniques*, Vol. 8, No. 3, 319–325, May 1960.
11. Nakano, H., Y. Shinma, and J. Yamauchi, "A monofilar spiral antenna and its array above a ground plane — Formation of a circularly polarized tilted fan beam," *IEEE Transactions on Antennas and Propagation*, Vol. 45, No. 10, Oct. 1997.
12. Chen, A., Y. Zhang, Z. Chen, and S. Cao, "A Ka-band high-gain circularly polarized microstrip antenna array," *IEEE Antennas and Wireless Propagation Letters*, Vol. 9, 1115–1117, 2010.
13. Insera, D., W. Hu, and G. Wenn, "Design of a microstrip series power divider for sequentially rotated nonuniform antenna array," *Int. Journal of Antennas and Propagation*, Vol. 2017, Article ID 9482979, 8 pages, 2017.
14. Tcheg, P. and D. Pouchè, "A design methodology for the implementation of planar spiral antennas with an integrated corporate feed," *Progress In Electromagnetics Research C*, Vol. 106, 239–253, 2020.

15. Chen, A., C. Yang, Z. Chen, Y. Zhang, and Y. He, "Design of multilevel sequential rotation feeding networks used for circularly polarized microstrip antenna arrays," *Int. Journal of Antennas and Propagation*, Vol. 2012, Article ID 304816, 2012.
16. Tcheg, P. and D. Pouhè, "K- and Ka-band Planar Spiral Antenna Arrays With Integrated Coplanar Feeding Network," *Progress In Electromagnetics Research C*, Vol. 113, 227–238, 2021.
17. Wu, Q., H. Wang, C. Yu, and W. Hong, "Low-profile circularly polarized cavity-backed antennas using SIW techniques," *IEEE Transactions on Antennas and Propagation*, Vol. 64, No. 7, 2832–2839, Jul. 2016.
18. Baghernia, E., M. Mamdouh, M. Ali, and A. Razik Sebak, " 2×2 slot spiral cavity-backed antenna array fed by printed gap waveguide," *IEEE Access*, Vol. 8, 170609–170617, Sep. 2020.